

Supplementary Information for

Unveiling the mechanism of improved capacity retention in $Pmn2_1$ $\text{Li}_2\text{FeSiO}_4$ cathode by cobalt substitution

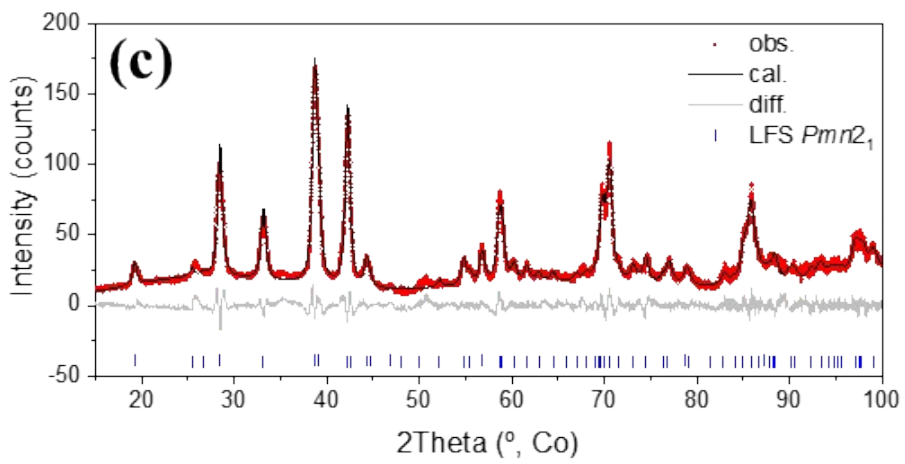
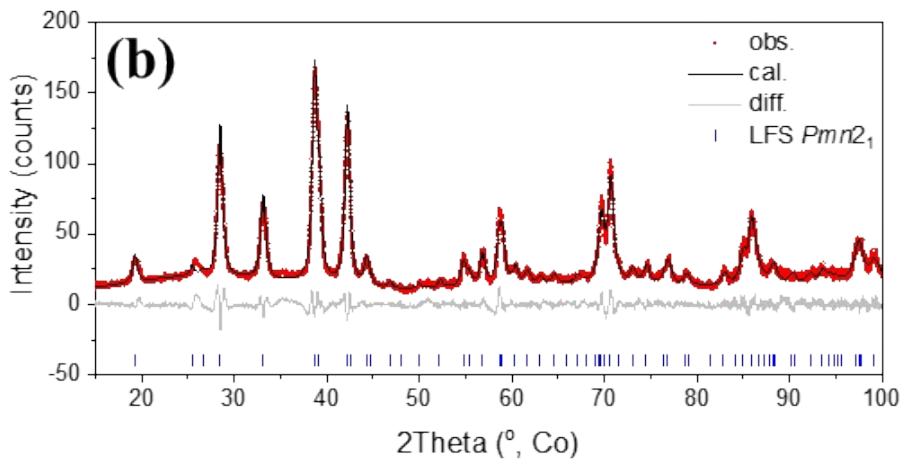
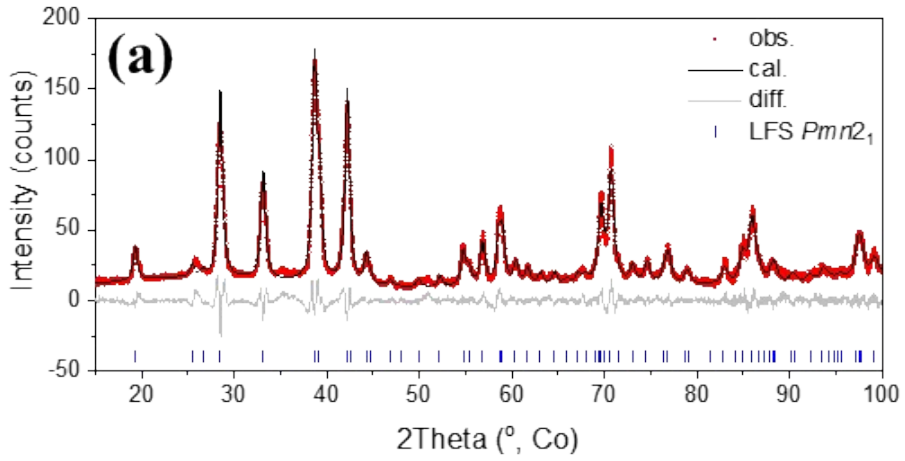
Yan Zeng¹, Hsien-Chieh Chiu¹, Bin Ouyang², Jun Song¹, Karim Zaghib³, George P.
Demopoulos^{1,*}

¹ Materials Engineering, McGill University, 3610 rue University, Montréal, QC H3A 0C5,
Canada

² Department of Materials Science and Engineering, University of California, Berkeley,
Berkeley, California 94720, United States

³ Centre d'excellence-ETSE, Hydro-Québec, Varennes, QC, Canada

* Corresponding author: ORCID #0000-0001-8112-5339, george.demopoulos@mcgill.ca



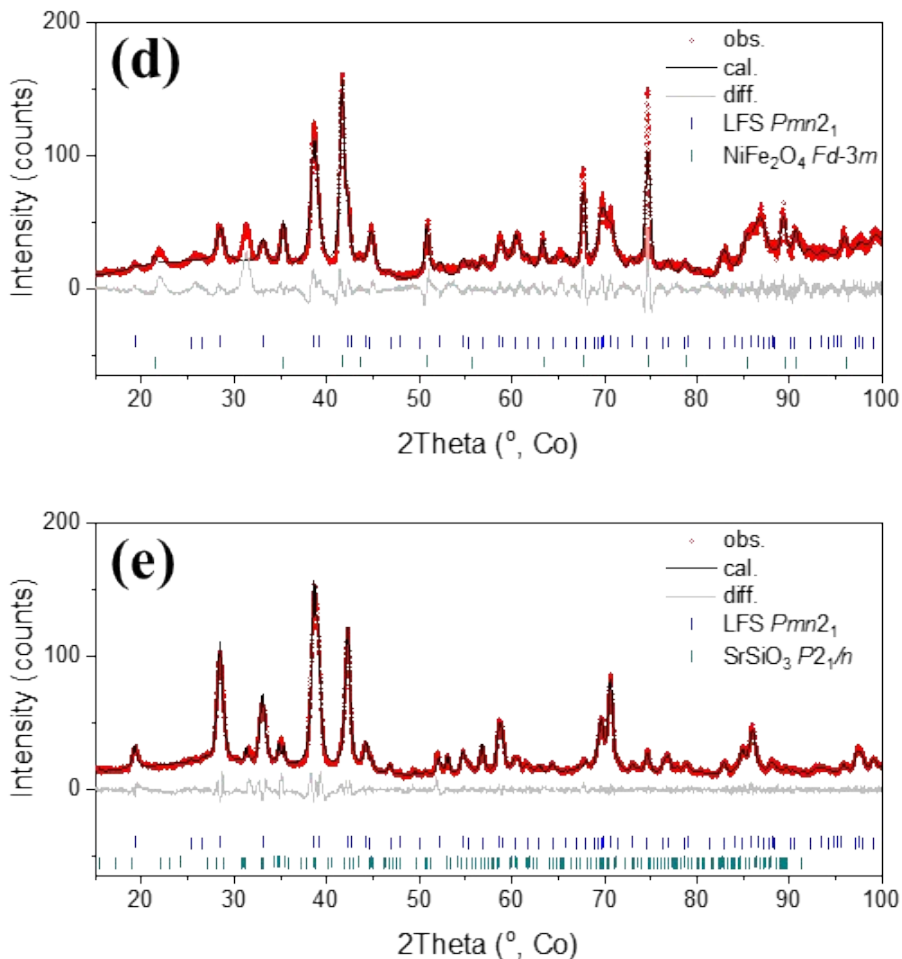


Figure S1. Le Bail refinement of powder X-ray diffractograms (Co-K α radiation, $\gamma = 1.7889 \text{ \AA}$) of Mg, Co, Ni, or Sr-involved $\text{Li}_2\text{FeSiO}_4$ (LFS) samples obtained by hydrothermal synthesis at 200°C . (a) Undoped LFS with determined lattice parameters of $a = 6.26873(21) \text{ \AA}$, $b = 5.33468(18) \text{ \AA}$, $c = 4.96970(18) \text{ \AA}$, and $V = 166.195(10) \text{ \AA}^3$. (b) Mg-LFS with determined lattice parameters of $a = 6.26586(23) \text{ \AA}$, $b = 5.33860(18) \text{ \AA}$, $c = 4.96815(18) \text{ \AA}$, and $V = 166.189(10) \text{ \AA}^3$. (c) Co-LFS with determined lattice parameters of $a = 6.25996(25) \text{ \AA}$, $b = 5.35188(19) \text{ \AA}$, $c = 4.96503(18) \text{ \AA}$, and $V = 166.341(11) \text{ \AA}^3$. (d) Ni-LFS with determined lattice parameters of $a = 6.27334(51) \text{ \AA}$, $b = 5.33224(42) \text{ \AA}$, $c = 4.97195(63) \text{ \AA}$, and $V = 166.316(28) \text{ \AA}^3$. (e) Sr-LFS with determined lattice parameters of $a = 6.27659(33) \text{ \AA}$, $b = 5.35413(27) \text{ \AA}$, $c = 4.96347(19) \text{ \AA}$, and $V = 166.801(14) \text{ \AA}^3$. Note that LFS, Mg-LFS, and Co-LFS were refined with a single phase of $\text{Li}_2\text{FeSiO}_4$ in orthorhombic S.G. $Pmn2_1$ (01-080-3671), whereas Ni-LFS was refined with $Pmn2_1$ $\text{Li}_2\text{FeSiO}_4$ and NiFe_2O_4 in cubic $Fd-3m$ (04-014-8286), and Sr-LFS was refined with $Pmn2_1$ $\text{Li}_2\text{FeSiO}_4$ and SrSiO_3 in monoclinic S.G. $P2_1/n$ (04-011-6968). The reported lattice parameters are for $Pmn2_1$ $\text{Li}_2\text{FeSiO}_4$ only. The refinement was performed using Academic TOPAS v.5.0 software.

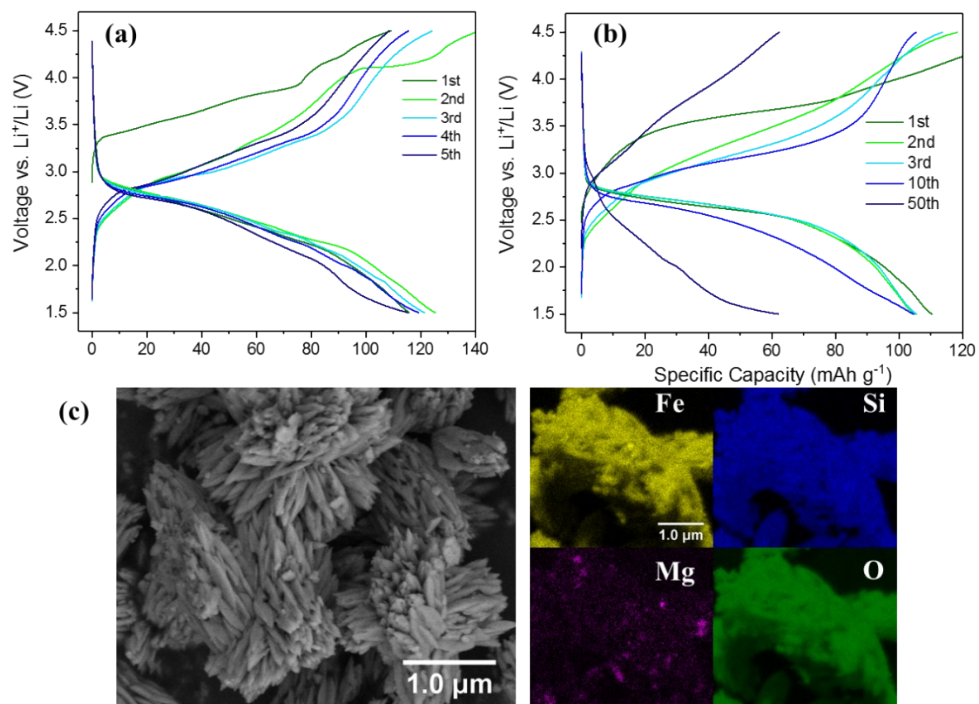


Figure S2. Galvanostatic charge-discharge curves of MgLFS at (a) C/30 and (b) C/10 between 1.5-4.5 V at 45°C. (c) SEM and EDS mapping of MgLFS.

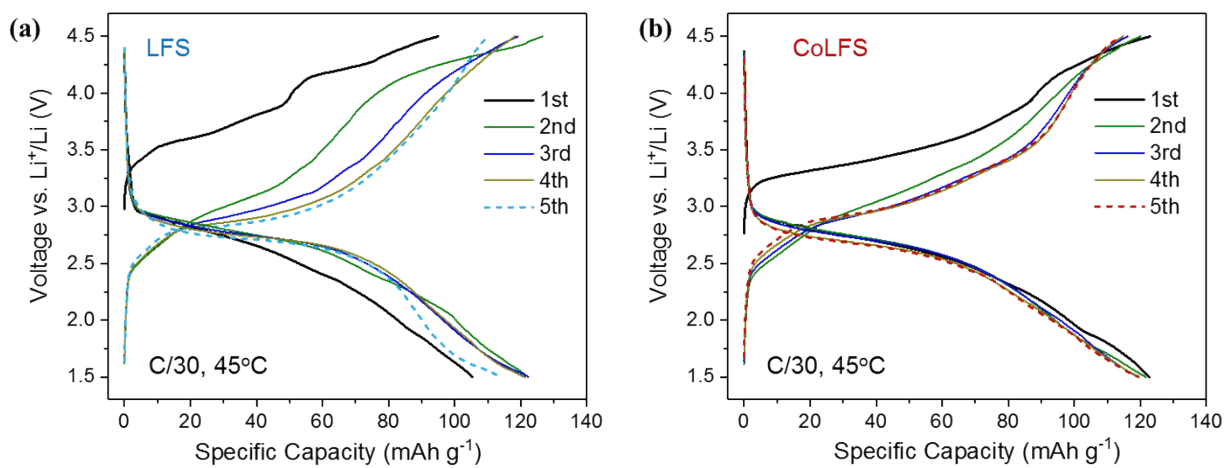


Figure S3. Galvanostatic charge-discharge curves of (a) LFS and (b) CoLFS at C/30 between 1.5-4.5 V at 45°C.

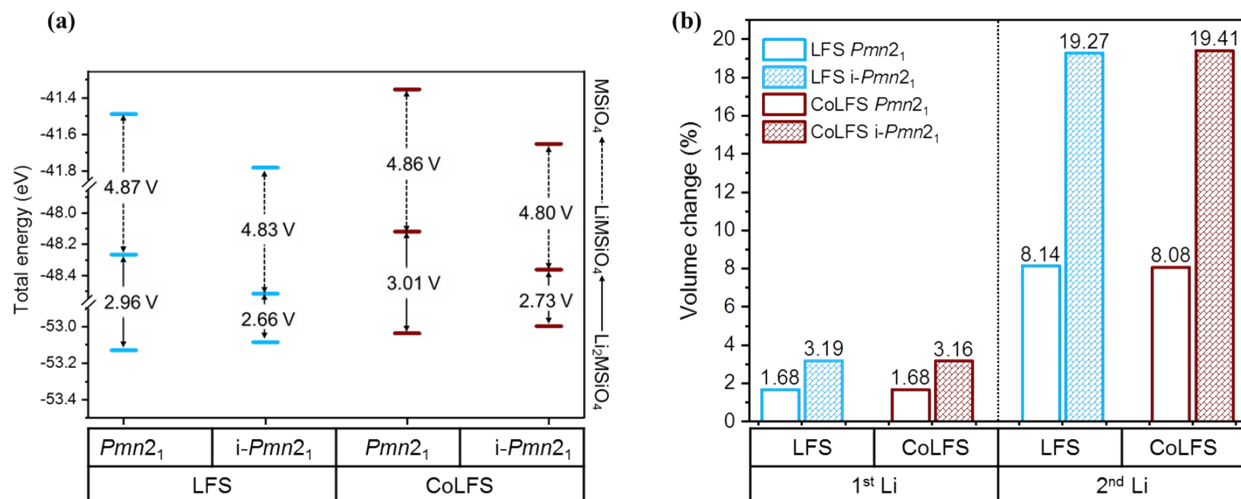


Figure S4. (a) Calculated total energies (eV/f.u.) of Li_2FeSiO_4 and $Li_2Fe_{0.94}Co_{0.06}SiO_4$ in $Pmn2_1$ and inverse- $Pmn2_1$ phases. (b) Calculated volume change (%) upon delithiation of $Li_yFe_{1-x}Co_xSiO_4$, where $y = 0, 1, \text{ or } 2$, x is the doping concentration of Co. Solid and open symbols represent $Pmn2_1$ and inverse- $Pmn2_1$ phases, respectively. It should be mentioned here that extraction of the second Li-ion will only occur at voltages above 4.8 V vs. Li^+/Li . The removal of the second Li, although has not been achieved in the present study, was found to exhibit pronounced volume change of over 19% after full delithiation to $FeSiO_4$ in inverse- $Pmn2_1$ structure. Structural arrangement and thereby profound volume change during charging-discharging will be one of the major obstacles to extract the second Li from Li_2FeSiO_4 . The strain caused by large volume change during electrochemical cycling would result in the failure of the cell. As the focus of the present work is to extract only the first Li, the volume change would not be an issue.

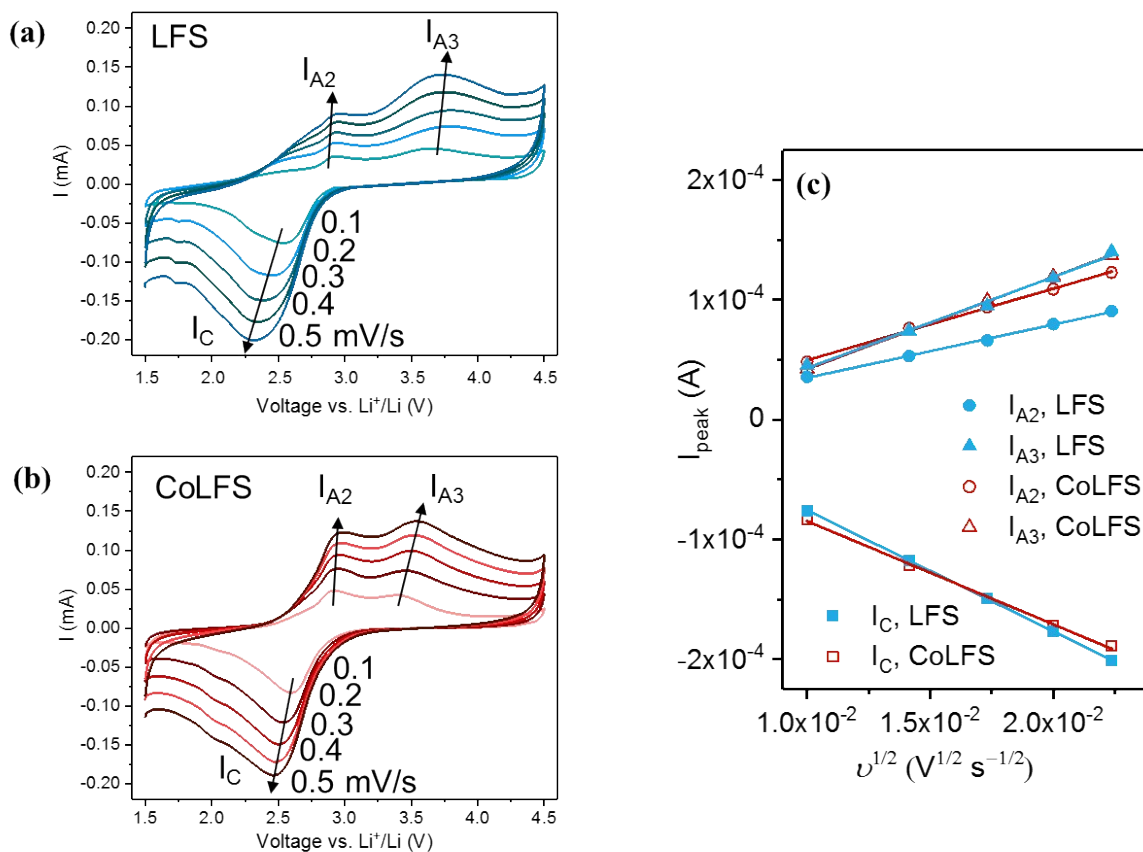


Figure S5. Cyclic voltammograms of (a) LFS and (b) CoLFS scanned at different rates from 0.1 mV s⁻¹ to 0.5 mV s⁻¹. I_{A2}, I_{A3}, and I_C represent two anodic peaks and one cathodic peak, respectively. (c) Fitting of the peak currents vs. the square root of scan rate.

Note to Figure S5:

Figures S5a and S5b show the variation of CV at various scan rates from 0.1 to 0.5 mV s⁻¹. Faster scan rate leads to a faster mass transport of Li⁺ and hence higher current can be obtained. Two anodic peaks and one cathodic peak can be observed despite the scan rate. The peak current, i.e., I_C, I_{A2}, or I_{A3}, is proportional to the square root of the scan rate v^{1/2}. The linear fitting results are shown in Figure S4c. Based on the Randles-Sevcik equation (eq S1) shown below, the chemical diffusion coefficient of Li⁺ can be estimated from the slope of the linear lines.^{S1-S2}

$$I_p = 0.4463 \left(\frac{F^3}{RT} \right)^{1/2} n^{3/2} A D_{Li^+}^{1/2} C_{Li^+}^* \nu^{1/2} \quad (S1)$$

where I_p is the peak current in A, F is the faraday's constant of 96,485 C mol⁻¹, R is the gas constant (8.314 J K⁻¹ mol⁻¹), T is the temperature in Kelvin, n is the number of electrons involved in the redox reaction, A is the surface area of the electrode in cm², D_{Li^+} is the chemical diffusion coefficient of Li⁺ in cm² s⁻¹, $C_{Li^+}^*$ is the initial concentration of Li⁺ in the bulk material in mol cm⁻³, ν is the scan rate in V s⁻¹. A is 0.785 cm². $C_{Li^+}^*$ is approximately 0.0386 mol cm⁻³ for the anodic reaction and 0.0201 mol cm⁻³ for the cathodic reaction. The calculated results of D_{Li^+} are listed in Table S4. As it can be seen, diffusion coefficient D_{Li^+} of I_C (lithiation) is larger than that of I_A (delithiation) for both LFS and CoLFS, while CoLFS has larger D_{Li^+} of I_A than LFS.

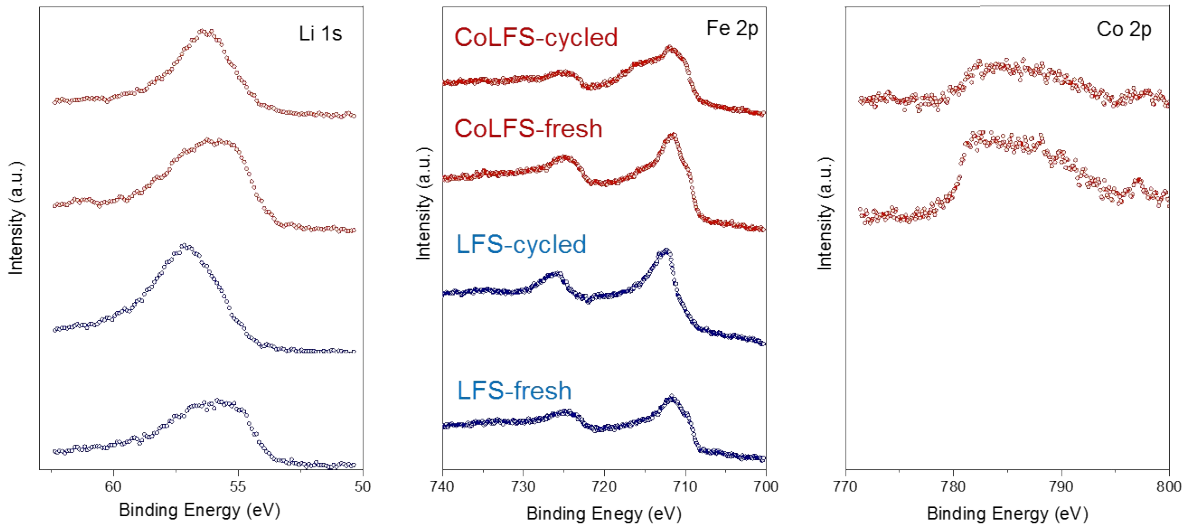


Figure S6. XPS spectra of Li 1s, Fe 2p, and Co 2p from the pristine and cycled electrodes of LFS and CoLFS (from bottom to top).

Table S1. Calculated total energies (eV/f.u.) of $\text{Li}_2\text{Fe}_{0.94}\text{M}_{0.06}\text{SiO}_4$ ($M = \text{Fe, Mg, Co, Ni, Sr, Ti, and Zr}$) in $Pmn2_1$ and inverse- $Pmn2_1$ phases

Compound	Total energy in $Pmn2_1$ (eV/f.u.)	Total energy in inverse- $Pmn2_1$ (eV/f.u.)
$\text{Li}_2\text{FeSiO}_4$	-53.13	-53.09
$\text{Li}_2\text{Fe}_{0.94}\text{Mg}_{0.06}\text{SiO}_4$	-53.03	-52.99
$\text{Li}_2\text{Fe}_{0.94}\text{Co}_{0.06}\text{SiO}_4$	-53.04	-53.00
$\text{Li}_2\text{Fe}_{0.94}\text{Ni}_{0.06}\text{SiO}_4$	-52.86	-52.77
$\text{Li}_2\text{Fe}_{0.94}\text{Sr}_{0.06}\text{SiO}_4$	-53.02	-52.96
$\text{Li}_2\text{Fe}_{0.94}\text{Ti}_{0.06}\text{SiO}_4$	-53.28	-53.24
$\text{Li}_2\text{Fe}_{0.94}\text{Zr}_{0.06}\text{SiO}_4$	-53.29	-53.25

Table S2. Calculated energies above the hull (meV/atom) and potential decomposition phases

Compound	Energy above the hull (meV/atom)	Decomposition phases
$\text{Li}_2\text{Fe}_{0.94}\text{Mg}_{0.06}\text{SiO}_4$	8.73	$\text{Li}_2\text{FeSiO}_4, \text{Li}_2\text{MgSiO}_4$
$\text{Li}_2\text{Fe}_{0.94}\text{Mn}_{0.06}\text{SiO}_4$	8.35	$\text{Li}_2\text{FeSiO}_4, \text{Li}_2\text{MnSiO}_4$
$\text{Li}_2\text{Fe}_{0.94}\text{Co}_{0.06}\text{SiO}_4$	8.65	$\text{Li}_2\text{FeSiO}_4, \text{Li}_2\text{CoSiO}_4$
$\text{Li}_2\text{Fe}_{0.94}\text{Ni}_{0.06}\text{SiO}_4$	12.10	$\text{Li}_2\text{FeSiO}_4, \text{Li}_2\text{SiO}_3, \text{NiO}$
$\text{Li}_2\text{Fe}_{0.94}\text{Sr}_{0.06}\text{SiO}_4$	14.57	$\text{Li}_2\text{FeSiO}_4, \text{Li}_2\text{SrSiO}_4$
$\text{Li}_2\text{Fe}_{0.94}\text{Ti}_{0.06}\text{SiO}_4$	33.03	$\text{Li}_2\text{FeSiO}_4, \text{Li}_2\text{SiO}_3, \text{Li}_2\text{TiSiO}_5, \text{Fe}$
$\text{Li}_2\text{Fe}_{0.94}\text{Zr}_{0.06}\text{SiO}_4$	583.19	$\text{Li}_2\text{FeSiO}_4, \text{Li}_2\text{SiO}_3, \text{ZrO}_2, \text{Fe}$

Table S3. Calculated cell voltage of $\text{Li}_2\text{FeSiO}_4$ and $\text{Li}_2\text{Fe}_{0.94}\text{Co}_{0.06}\text{SiO}_4$. The absolute values of cell voltage calculated in this work are 0.1-0.3 V lower than those reported in the literature, which can be attributed to different effective Hubbard U and total energy of Li metal used in the calculations

Compound	Phase	Cell voltage E (V vs. Li^+/Li)	ref.
$\text{Li}_2\text{Fe}_{1-x}\text{Co}_x\text{SiO}_4 \rightarrow \text{LiFe}_{1-x}\text{Co}_x\text{SiO}_4$			
$\text{Li}_2\text{FeSiO}_4$	$Pmn2_1$	2.96	this work
		3.10	Soe <i>et al.</i> ^{S3}
		3.34	Eames <i>et al.</i> ^{S4}
	inverse- $Pmn2_1$	2.66	this work
		2.82	Soe <i>et al.</i> ^{S3}
		2.83	Saracibar <i>et al.</i> ^{S5}
		3.04	Eames <i>et al.</i> ^{S4}
$\text{Li}_2\text{Fe}_{0.94}\text{Co}_{0.06}\text{SiO}_4$	$Pmn2_1$	3.01	this work
	inverse- $Pmn2_1$	2.73	this work
$\text{LiFe}_{1-x}\text{Co}_x\text{SiO}_4 \rightarrow \text{Fe}_{1-x}\text{Co}_x\text{SiO}_4$			
LiFeSiO_4	$Pmn2_1$	4.87	this work
		4.86	Saracibar <i>et al.</i> ^{S5}
	inverse- $Pmn2_1$	4.83	this work
		4.80	Soe <i>et al.</i> ^{S3}
		4.82	Saracibar <i>et al.</i> ^{S5}
$\text{Li}_2\text{Fe}_{0.94}\text{Co}_{0.06}\text{SiO}_4$	$Pmn2_1$	4.86	this work
	inverse- $Pmn2_1$	4.80	this work

Table S4. Chemical diffusion coefficient D_{Li^+} of LFS and CoLFS calculated from cyclic voltammetry measurements.

Electrode	Peak	Slope of I_p vs. $v^{1/2}$	D_{Li^+} , cm^2/s
$\text{Li}_2\text{FeSiO}_4$	I_C	0.0101	6.07×10^{-12}
	I_{A2}	0.0045	3.20×10^{-13}
	I_{A3}	0.0076	9.30×10^{-13}
$\text{Li}_2\text{Fe}_{0.94}\text{Co}_{0.06}\text{SiO}_4$	I_C	0.0086	4.41×10^{-12}

I _{A2}	0.0060	5.74×10^{-13}
I _{A3}	0.0077	9.55×10^{-13}

Table S5. Binding energies (eV) and atomic percentages (%) of C, O, F, P, and Si from XPS spectra of the pristine and cycled electrodes of LFS and CoLFS

	binding energy, eV	LFS-pristine, eV	%	LFS-cycled, eV	%	CoLFS-pristine, eV	%	CoLFS-cycled, eV	%
C 1s			53.7		39.7		50.9		32.3
C-C	284.8	284.8	16.4	284.8	10.4	284.8	17.2	284.8	9.9
CH ₂	~286	286.1	27.1	286.1	17.4	285.9	25.2	286.7	19.1
O-C=O	~288.5	289.2	2.2	287.6	5.9	289.2	2.1	289.7	0.1
CF ₂	~292	291.1	8.0	290.9	5.0	291.1	6.4	291.0	3.2
O 1s			25.7		32.2		29		33.6
Li-O, Fe-O, Co-O	529-530	531.2	15.7	531.6	15.6	531.2	17.5	531.4	7.9
C-O, CO ₃ , SiO ₄	531.5-532	532.6	10.0	532.7	11.3	532.7	11.5	532.6	18.9
P-O	534			534.1	5.3			534.0	6.8
F 1s			14.8		19.2		12.9		24
LiF	684-685.5	685.3	1.4	685.5	7.2	685.4	1.2	685.5	13.6
CF ₂ , Li _x PO _y F _z	688.8-689	688.2	13.4	687.9	12.0	688.2	11.7	688.1	10.4
P 2p									
Li _x PO _y F _z	135		0	135.1	3.6		0	135.3	5.9
Si 2p									
SiO ₄ , Si-F	101.6-103.8	102.2	5.9	102.6	5.5	102.3	7.3	102.9	4.2

Note to Figure 5:

CV deconvolution (Figures 5c and 5d) was performed with the pre-assumptions:

- 1. The I-V response follows the behaviours of thin-layer cyclic voltammetry where the bell-shaped (gaussian) curve applies. This is supported by the architecture of electroactive LFS as it is confined in the tens-of-micrometer space between the separator and Al current collector.*
- 2. The redox reactions are exclusively from ferrous/ferric couple existing in LFS crystals.*
- 3. Peak position reflects the coordination environment around Fe atoms in the crystal structure. Thus, different structure leads to different peak positions as reported by Sirisopanaporn et al.^{S6}*
- 4. LFS crystals are connected in parallel in the electrode.*

In this context, each peak in cyclic voltammograms corresponds to a particular Li-ion intercalation process of the corresponding intermediate phase of LFS; the integrated intensity of the peak is related to the concentration of the electroactive ferrous/ferric couples in LFS. Hence, the newly formed intermediate LFS can be estimated through the peak area. It is worth mentioning that there exist almost infinite combinations of the peak selection, just like the equivalent circuit model for EIS. Therefore, only the most outstanding four peaks were selected for the peak deconvolution.”

References

- S1. Elgrishi, N.; Rountree, K. J.; McCarthy, B. D.; Rountree, E. S.; Eisenhart, T. T.; Dempsey, J. L., A practical beginner's guide to cyclic voltammetry. *Journal of Chemical Education* **2018**, *95* (2), 197-206.
- S2. Zhu, Y.; Gao, T.; Fan, X.; Han, F.; Wang, C., Electrochemical techniques for intercalation electrode materials in rechargeable batteries. *Accounts Chem Res* **2017**, *50* (4), 1022-1031.
- S3. Seo, D.-H.; Kim, H.; Park, I.; Hong, J.; Kang, K., Polymorphism and phase transformations of $\text{Li}_{2-x}\text{FeSiO}_4$ ($0 \leq x \leq 2$) from first principles. *Physical Review B* **2011**, *84* (22), 220106.
- S4. Eames, C.; Armstrong, A. R.; Bruce, P. G.; Islam, M. S., Insights into changes in voltage and structure of $\text{Li}_2\text{FeSiO}_4$ polymorphs for lithium-ion batteries. *Chemistry of Materials* **2012**, *24* (11), 2155-2161.
- S5. Saracibar, A.; Van der Ven, A.; Arroyo-de Dompablo, M. E., Crystal structure, energetics, and electrochemistry of $\text{Li}_2\text{FeSiO}_4$ polymorphs from first principles calculations. *Chemistry of Materials* **2012**, *24* (3), 495-503.
- S6. Sirisopanaporn, C.; Masquelier, C.; Bruce, P. G.; Armstrong, A. R.; Dominko, R., Dependence of $\text{Li}_2\text{FeSiO}_4$ electrochemistry on structure. *Journal of the American Chemical Society* **2011**, *133* (5), 1263-1265.